

THE GAMMA-RAY BLAZAR CONTENT OF THE NORTHERN SKY

DAVID SOWARDS-EMMERD¹, ROGER W. ROMANI & PETER F. MICHELSON¹Department of Physics, Stanford University, Stanford, CA 94305-4060
dse@darkmatter.stanford.edu, rwr@astro.stanford.edu, peterm@stanford.edu*ApJ submitted*

ABSTRACT

Using survey data, we have re-evaluated the correlation of flat spectrum radio sources with *EGRET* sources in the Northern sky. An analysis incorporating the radio and X-ray properties and the γ -ray source localization is used to gauge the reliability of associations and to search for counterparts of previously unidentified *EGRET* sources. Above $|b|=10^\circ$, where the classification is complete, we find that 70% of the Northern *EGRET* sources have counterparts similar to the bright *EGRET* blazars. For several of these we identify known blazar counterparts more likely than the earlier proposed 3EG association; for ~ 20 we have new identifications. Spectroscopic confirmation of these candidates is in progress and we have found flat spectrum radio quasars and BL Lac counterparts with redshifts as high as 4. We also find strong evidence for a set of 28 objects with no plausible counterpart like the known *EGRET* blazars. These thus represent either a new extragalactic population or a population of Galactic objects with a large scale height. The survey has been extended into the plane, where we find several new blazar candidates; the bulk of the sources are, however, Galactic. Looking ahead to the GLAST era, we predict that several of the present 3EG sources are composite and that higher resolution data will break these into multiple blazar IDs.

Subject headings: AGN: blazars – surveys: radio – surveys: optical – Gamma Rays

1. INTRODUCTION

The *EGRET* telescope on the *CGRO* satellite has detected 271 sources in a survey of the Gamma-ray (~ 100 MeV to 10 GeV) sky. Of these roughly a quarter have been identified as blazars and along the Galactic plane there are a half dozen objects confirmed as young pulsars through their pulsed γ -ray emission. Thus the bulk of the sources remain to be identified. There is a young Galactic population along the plane clearly correlated with high mass stars (Kaaret & Cottam 1996; Yadigaroglu & Romani 1997). An intermediate latitude excess, especially in the direction of the Galactic bulge, suggests an older Galactic population whose nature is uncertain. Finally there remain a substantial number of high latitude sources with no AGN identification.

The selection of blazar candidates has largely proceeded by correlation with existing radio surveys (Hartman *et al.* 1999; Mattox *et al.* 2001). In contrast, the Galactic plane sources and individual intermediate latitude sources have been the subject of targeted multi-wavelength campaigns (Roberts, Romani & Kawai 2001; Halpern *et al.* 2001; Wallace *et al.* 2002). In this project we attempt to obtain a more complete census of plausible blazar counterparts, sifting sources with extant radio survey data and then conducting a multi-wavelength follow-up. We are obtaining spectroscopic confirmation of the candidate AGN with Hobby-Eberly Telescope (HET) Marcario LRS spectroscopy. This survey has already discovered a number of new likely γ -ray blazars, including good candidates for the most distant persistent γ -ray sources known.

1.1. *Blazar Properties*

The ‘blazar’ label is somewhat heterogeneous, but in the context of the unified AGN model, these sources are

¹ also, Stanford Linear Accelerator Center, Stanford, CA, 94039-4349

believed to be viewed close to the axis of a powerful relativistic jet. As such they are compact flat spectrum radio sources, with apparent superluminal motion at VLBI scales. The optical counterparts exhibit significant polarization and OVV (optically violently variable) behavior (Urry & Padovani 1995). Optical spectroscopy often shows large equivalent width emission lines (flat spectrum radio quasars) while a significant fraction are continuum-dominated BL Lac-type objects. The broad-band spectral energy distribution (SED) is sometimes used to divide these into two classes with ‘red’ blazars showing a synchrotron peak in the IR-optical with a Compton peak in the γ -ray while ‘blue’ blazars have a synchrotron component extending into the X-ray with a Compton peak inferred to extend to the TeV range (Urry 1999, and references therein). There are surveys underway to substantially increase the number of known blazars (e.g. DXRBS; Landt *et al.* 2001) which will eventually help in systematizing the broad-band properties of these sources.

Of these properties bright, flat spectrum radio emission seems best correlated with γ -ray activity, but this may be primarily a selection effect of present counterpart lists, which focused on the brightest radio sources as the principal candidates. In an effort to make a less biased census of the counterparts, we have re-examined the correlation with X-ray and radio properties in selecting candidates.

2. COUNTERPART SELECTION AND ‘FIGURE OF MERIT’ RANKING

The existing γ -ray blazar lists were largely selected from the Green Bank 6cm and 21cm single dish surveys (Condon, *et al.* 1991; White & Becker 1992). With relatively poor resolution, confusion and extended jet/host galaxy

emission were a serious impediment to selecting flat spectrum cores as blazar counterparts. This was especially true at lower radio fluxes and toward the Galactic plane. Accordingly few sub-Jy counterparts have been identified. Real progress can now be made since interferometric surveys covering much of the Northern sky are available at 21cm (NVSS; Condon, *et al.* 1988) and 3.5cm (CLASS; Myers, *et al.* 2002 – the source list was kindly supplied in advance of publication by Ian Browne). The CLASS survey, targeting compact gravitational lens candidates, pre-selected flat spectrum sources by comparing NVSS 21cm and Green Bank single dish 6cm fluxes, mapping sources with spectral index $\alpha \leq 0.5$ ($S_\nu \propto \nu^{-\alpha}$) with the VLA A array, to resolve structure at the $0.2''$ scale. Coverage was complete for $\text{Dec} \geq 0^\circ$ and $|b| \geq 10^\circ$; there was also partial coverage beyond these limits. We are primarily interested here in the isolated unresolved cores that are not lens candidates.

By comparing the 3.5cm and 21cm interferometric fluxes we have a greatly improved estimate of the spectral index of the compact cores, which are well identified by sub-arcsecond positional matches. We find that a number of sources previously selected as ‘flat’ have extended high frequency emission. Of course with such a variable population, non-simultaneous observations can have erroneous spectral indices, but our estimates are certainly much better than extrapolations from the confused GB6 fluxes.

When CLASS coverage is not available, we do need to use GB6 fluxes. Following the CLASS prescription, we subdivide the 6cm flux between the coincident 21cm NVSS sources to make spectral index estimates. We then extrapolate with the 4.85GHz/1.4GHz spectral index to 8.4GHz to estimate a flux in the CLASS range. In general, this extension was needed in the Galactic plane where a plethora of 21cm sources make spectral indices unreliable. However, in a number of cases we are able to show that no target meets the CLASS survey criterion in the *EGRET* error box. This will be used to rule out typical blazar-type counterparts. All sources classified as blazars ended up having a CLASS detection, except 3EG J2016+3657.

We augment this radio selection by using the convenient, relatively uniform RASS bright and faint source catalogs. Counterpart candidates are evaluated for suitability of optical follow-up with USNO-B1.0/POSS photometry. Our analysis will use the positions of these counterparts in the ‘Test Statistic’ (TS) maps of the Third *EGRET* (3EG) catalog, which plot the estimated likelihood of the observed γ -rays as a function of point source location.

2.1. Radio/X-ray properties

High frequency radio emission is clearly a good discriminant. However to make the least biased selection of counterparts, we compute the over-density of sources near high latitude ($|b| > 20^\circ$) gamma-ray detections in bins of radio flux, spectral index and x-ray flux. To do this, we compare the number of sources detected within a given TS probability contour with many random realizations of the sky. The latter were obtained by shifting the *EGRET* TS maps on the sky in 2 degree increments, computing the random source TS values and correcting for variation in sky area from the survey cuts. The source counts within a given confidence contour as a function of, e.g., 8.4GHz

flux, were then compared to the random realizations after normalization by the effective sky coverage. We define the excess fractional source density associated with the 3EG source as

$$n = \frac{N_{3EG} - N_{Random}}{N_{3EG}} \quad (1)$$

for each flux bin. The distribution for 8.4 GHz flux within the 95% confidence region is shown in figure 1. A simple least-squares power law fit to the binned data then defines our excess source density function for evaluation of individual candidates. This exercise shows significant excess at fluxes well below the \sim Jy limit considered in earlier analyses. Other authors have also recently concluded that fainter radio sources should be considered as plausible candidates (Wallace *et al.* 2002).

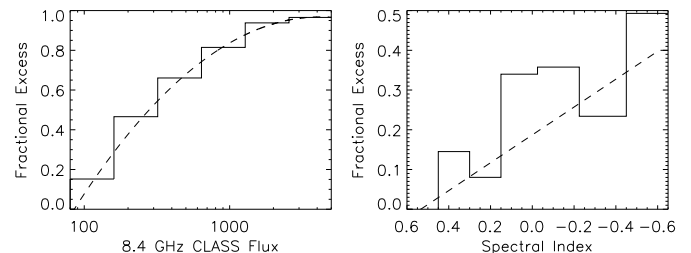


FIG. 1.— The excess fractional source density within *EGRET* 95% error contours as a function of: 8.4 GHz (CLASS) flux (left), and 1.4GHz/8.4GHz spectral index (right).

We have similarly measured the excess of flat spectrum sources as a function of spectral index. Here the correlation is strongest for $\alpha \lesssim -0.6$, becoming negligible for $\alpha \geq 0.53$. Correlation with the RASS source catalog also shows an excess. However the maximum excess for the brightest sources is only 0.5 and about half of the strong radio counterpart candidates were not detected in the relatively shallow all-sky survey (some are present in deeper pointed observations). Clearly we do not wish X-ray non-detection to exclude a candidate, although X-ray bright sources are somewhat more likely to be correlated with the *EGRET* detections. We thus add 0.5 to the best fit X-ray n so that it runs from 0.5 to 1.0. In this way X-ray detection can increase the source’s selection by up to a factor of 2 (for $>1\text{PSPC}$ cps), but X-ray non-detection is not seriously constraining. Thus the X-ray component of our analysis is not crucial – if it is excluded no sources are lost from our final source list, although their detailed ranking does change somewhat. The excess probability functions exhibited no strong dependence on the gamma-ray source localization. Therefore, the area within the 95% contours were taken to be representative of the gamma-ray sky for the derivation of the merit functions.

2.2. Source Position Weighting

The combination of 8.4GHz flux, spectral index and X-ray flux provides a useful tool for identifying *EGRET*-like blazars. Indeed, we are studying a set of objects selected by these cuts, without any 3EG coincidence, as possible GLAST-detectable blazars. Given the strong γ -ray variability and the limited duty cycle in the flaring state, it would not be very surprising for relatively bright sources to have eluded detection during the limited *EGRET* exposure. However, to select *individual EGRET* counterparts, we will also use the radio source position in the likelihood

analysis. Previous blazar identification efforts have used the circular or elliptical fits to the TS maps as an approximation to the allowed sky region. However, many TS maps contain open or complex contours at the 95% level, so we employ instead the precise TS at the radio source position.

The value at our counterpart candidate position (α, δ) is compared to the map maximum, giving $\Delta TS = TS_{max} - TS(\alpha, \delta)$. ΔTS has been calibrated by Monte Carlo simulations (Mattox *et al.* 1996) to give the statistical probability $L[\Delta TS(\alpha, \delta)]$ that the source lies within the contour of constant ΔTS for 50%, 68% 95% and 99% confidence levels. We linearly interpolate between these values to obtain a smooth $L[\Delta TS(\alpha, \delta)]$; sources at large ΔTS have little probability of association with the 3EG source, even if very blazar-like. The statistical error estimate for ΔTS does not, however, account for position uncertainties associated with nearby unmodeled γ -ray sources and with other systematic and instrumental biases. This is confirmed by plotting the distribution of bright 3EG blazars (Mattox *et al.* 2001) as a function of ΔTS . Considerably fewer than half of the sources lie within the 50% contour, and several lie outside the 99% contour. We find that the additional spread can be well modeled by dividing the map value of ΔTS by 1.5 and then computing the nominal statistical positional probability. The probabilities renormalized in this way are a good match to the observed source distribution.

2.3. Combined Figure of merit

We combine the fractional excesses for each of the counterpart candidate’s properties with the estimate of the positional probability to compute a total ‘Figure of Merit’ for the source as a radio/X-ray counterpart:

$$FoM = n_{8.4GHz} \times n_{\alpha} \times n_{x-ray} \times L(\alpha, \delta) \quad (2)$$

Notice that this product of excess source fraction and positional uncertainty is *not* a normalized probability of source identification. It is however an unbiased ranking of the counterpart likelihood that can be compared across the entire (high latitude) 3EG population. To avoid confusion, we multiply by 100 in the quoted FoM values.

To evaluate the significance of this FoM statistic, we produced random realizations of the radio/X-ray sky by random, independent RA and DEC draws from the true CLASS position list, after excluding the actual positions of the ~ 70 highest-FoM coincident sources [which would otherwise imprint the observed correlation on the random realizations]. We compute the average distribution of FoM for 10^3 realizations of such random skies, and compare with the true FoM distribution in Figure 2. The hashed region shows the $\pm 1\sigma$ range for our estimate of the fraction of sources in a given FoM bin that are ‘real’, i.e. in excess of random coincidence. For $FoM < 0.1$ there is little excess correlation. There is a puzzling deficit of true sources with $FoM \sim 2$, but we have not been able to trace this to any one of the FoM source properties and so conclude that this is a statistical fluctuation. We select sources with $FoM \geq 0.25$ (i.e. $< 20\%$ false positive, even for the lowest FoM) as good counterparts; this is about a factor of two above the lowest bins showing significant correlation. To facilitate comparison with earlier ID lists, we divide these sources in half with $FoM > 1$ designated as ‘likely’

counterparts and $0.25 < FoM < 1.0$ as ‘plausible’ counterparts (note however that our ‘plausible’ sources have a relatively high fraction of true associations). The line in figure 2 shows a simple linear fit to the source probability with a strong decrease below $FoM=0.1$. Integrating through the distribution of measured FoM, we find that of the 35 ‘likely’ sources we expect less than 3 false positives ($\geq 92\%$ good IDs) and of the 32 ‘plausible’ sources ≤ 6 may be false positives ($\geq 82\%$ good IDs). We can compare the FoM distributions of our IDs with those designated in the 3EG catalog and in Mattox *et al.* (2001). Many of the highest FoM sources are common to all lists. However, both the 3EG and Mattox lists claim high confidence for several sources that we only assign low probability. In addition each list has a number of sources that are not flat spectrum or compact and do not meet our interferometric selection criteria. These sources, 11 in the 3EG and 7 in Mattox *et al.* (2001) are mostly lower confidence (‘a’ and ‘plausible’ designations in these catalogs). However, in addition to selecting previous IDs, we also find $\sim 50\%$ more high confidence sources than either, and virtually all of our ‘plausible’ sources are new. Noting that Mattox *et al.* (2001) retained ‘plausible’ sources with estimated likelihoods as low as a few percent, while our lowest FoM sources have a likelihood $> 80\%$, we believe that our list is less biased, more complete and more reliable than earlier efforts. In particular, we can more easily identify multiple associations with a given *EGRET* source, rather than taking only the ‘best’ blazar ID.

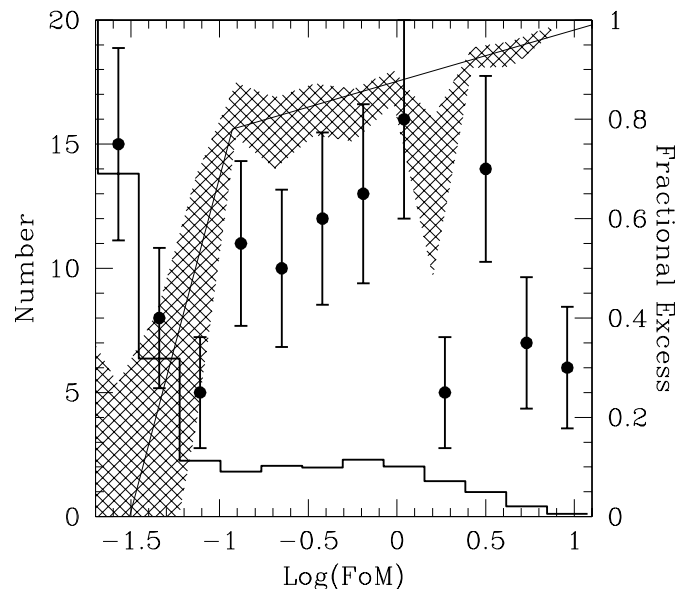


FIG. 2.— Random (histogram) and true (points, with Poisson error bars) distributions of our FoM. The fractional excess (true ID fraction) for each bin is shown by the (Poisson) error range of the shaded region (right scale). Note the rapid fall-off of reliable identification below $\text{Log}(FoM) \approx -0.9$.

2.4. Radio Counterpart IDs

We find at least one blazar candidate counterpart for 66 of the Northern 3EG sources. In many cases, the previously claimed 3EG ‘high confidence’ and ‘plausible’ blazars are recovered with the largest FoM value for a given error ellipse. However, in a number of cases, our criteria select a different blazar as much more likely than the claimed

catalog association. In addition, we find some 2 dozen new radio associations in the Northern sky, whose FoM confidence are at least as good as that of the lowest of the previously identified ‘high confidence’ sources. In several cases there are multiple radio blazar IDs in a single *EGRET* error ellipse. One rather complex example is 3EG J0118+0248. In the 3EG catalog this was possibly identified with 0119+041; our analysis does select it as a (low FoM) possible association, but it is well outside the 99% error contour. In the Mattox *et al.* (2001) analysis, the 3EG source was attributed to 3C37 ($z = 0.672$); this AGN however has a quite steep spectrum for the compact component and does not meet our blazar identification criteria. Instead, our analysis selects two compact flat spectrum sources as the most likely counterparts. The first is a relatively low luminosity radio galaxy core at $z=0.047$, the second is a newly discovered flat spectrum radio QSO at $z=4.0$. The 3EG error contours are quite elongated with the major axis spanning these two sources (Figure 3), although 0119+041 is also a plausible source of this extension. A second example is 3EG J0808+5114, which hosts a flat spectrum radio quasar at $z=1.14$ and a BL Lac at $z=0.13$, again separated along the major axis of an extended γ -ray uncertainty region. Given that the 3EG survey is strongly flux limited, that the γ -ray blazar luminosity function is quite steep, and that the poor γ -ray resolution causes substantial source overlap and confusion, it is not surprising that in some cases a combination of fainter sources can push a location above the detection threshold. In several other cases support for multiple IDs comes from complex or elongated likelihood (‘TS’) maps.

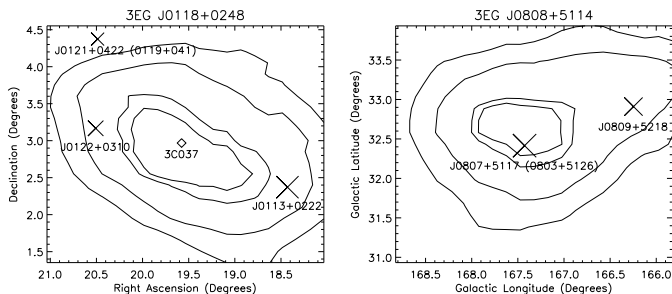


FIG. 3.— TS maps of possible composite 3EG sources. Left 3EG J0118+0248. The 3EG identification 0119+041, the steep spectrum Mattox *et al.* (2001) counterpart 3C037 (diamond) and our two new blazar counterparts (along the uncertainty region major axis) are shown. Right: 3EG J0808+5114. Again two high confidence identifications lie along the major axis.

2.5. Radio non-IDs

Since the GB6/NVSS/RASS provide a uniform survey (abetted by CLASS follow-up), the absence of plausible IDs for some *EGRET* sources is significant. For example, we find no IDs for two high latitude sources believed to be likely pulsars (3EG J0010+7300= CTA 1 and 3EG J1835+5918, see Reimer *et al.* 2001). Our technique allows us to select *individual* 3EG sources as non-blazar IDs. This is particularly useful at intermediate latitude, as it lets us separate the blazar fraction of the population, leaving a cleaner non-blazar sample. North of Dec=0°, 28 previously unidentified sources are selected as *not* like *EGRET* blazars. There is some concentration to the Galactic plane, but much of this sample is at high latitude, suggesting either a new class of extragalactic γ -ray

sources or an old high scale height Galactic populations of pulsars or similar objects.

2.6. Summary Results

We summarize our source classification in Table 1 and Figure 4. In summary, of the 116 Northern 3EG sources (excluding the Solar flare), 66 have at least one plausible blazar-like radio counterpart. In the Table our high confidence associations are listed in bold face and our lower confidence associations in plain text. Previously claimed AGN associations not supported by our analysis are given in italics in parentheses, with FoM values computed when possible. The Table also notes 10 sources associated with pulsars or known plerion/young SNR (indented). These are neutron star/pulsar/SNR associations from the 3EG catalog, with a few additions from new discoveries which are noted in the individual source comments. Of course many additional associations have been claimed for Galactic objects; we do not evaluate or exhaustively review these here, but we believe that beyond the few pulsed detections, the identifications rapidly become quite speculative.

An additional 28 sources are unidentified but according to our analysis are definitively unlike the known 3EG blazars. The remaining sources are at low $|b| \leq 5^\circ$ latitude. Only faint flat spectrum sources are allowed in the error boxes of 7 of these and, given the high density of Galactic sources, these are almost certainly chance coincidence. The final 5 show bright extended HII regions which could, in principal, hide a bright flat spectrum compact blazar, but again in practice we expect the sources to be Galactic. Further radio imaging study could better rule out AGN counterparts in these cases.

Figure 4 summarizes the present 3EG source classifications in Galactic coordinates. Above the Dec=0 line, we use our new classifications from Table 1, with blazars as filled circles. In the South, the same symbols are used for the 3EG ‘A’ and ‘a’ blazar designations. Pulsar IDs and strong pulsar/plerion candidates are shown by filled and open stars. The definitive non-blazars are shown by open circles. The improved completeness of the Northern classification is evident. Clearly pushing south into the bulge population will be very interesting.

Since AGN are expected to be isotropic, it is of interest to examine the distribution of the northern blazar IDs. Detailed comparison requires folding through the *EGRET* exposure and sensitivity maps for a model blazar luminosity function; we defer this to a future communication. However since exposure is relatively uniform for $|b| > 20^\circ$, we report simple number counts. From $30^\circ < |b| < 90^\circ$ we find 36 blazar identifications, or 11.6/sr within our survey boundary. Extrapolating toward the plane, we find for $20^\circ < |b| < 30^\circ$ 12 sources against 11 expected. At $10^\circ < |b| < 20^\circ$ we find 8 sources vs. 12 expected, and a similar fraction within 10° of the plane. Given the higher background and detection threshold near the plane, this does not however mean that our identification of blazars at low $|b|$ is incomplete.

3. OPTICAL FOLLOW-UP

Of our radio-selected counterparts, 50 are new sources, not selected in previous *EGRET* counterpart lists. Further, several additional selected radio sources, while flagged as possible counterparts in earlier studies, have not had spectroscopic confirmation of their AGN nature. We first checked for published spectroscopy of these radio sources, comparing with the Tenth Edition of the Quasar Catalog (Veron-Cetty *et al.* 2001) and cross checking by querying NED. We find that 16 (5 high probability IDs) of our newly selected counterparts have known redshifts. However over thirty sources in the Northern sky were found to have previously unstudied blazar-like radio/X-ray candidate counterparts, many with quite high FoM. These are the target of our HET spectroscopy, along with a number of similar sources having no *EGRET* association.

Just before submission, we learned that Halpern, Eracleous & Mattox (2003) have recently completed follow-up spectroscopy of a set of previously claimed radio counterparts of 3EG (and 2EG, GEV) sources with lower 4.8GHz fluxes. Their list includes 8 sources also identified in our exercises. For three sources we have new spectroscopy in common; for two their new redshift agrees with that which we obtain (below). We were also able to obtain a redshift for the third source (J1826+0149). For three other sources Halpern, Eracleous & Mattox (2003) obtain no z , for two the z they measure was already found in the QSO catalog, and for the last (J1239+0443) they obtain a new z . This value is included in our table as the only entry not from cataloged data or our new spectroscopy.

3.1. HET LRS Spectroscopy

Spectroscopy was obtained using the Marcario Low Resolution Spectrograph (LRS)(Hill *et al.* 1998) on the 9.2m HET (Ramsey *et al.* 1998). This novel telescope, of tilted optical Arecibo design is still under development, but with a range of magnitudes the blazar candidates were suitable targets for the early operations phase. These targets were observed in regular queue observations from 3/02 -2/03. We obtained 2×450 s exposures for most targets; a few of the most interesting fainter targets were observed with 2×900 s exposure. Observations were made employing a 300 l/mm grating and a $2''$ slit for a dispersion of 4\AA per (binned) pixel and an effective resolution of 16\AA covering $\lambda\lambda 4200 - 10500$. The new spectra are displayed in Figure 5.

Standard IRAF CCD reductions, optimal extraction and calibration were performed. Unfortunately, the varying pupil during the HET tracks is not yet fully monitored and so small (few %) flat-field variations were not corrected, as with untracked flat field frames the varying illumination worsened the (already substantial) fringe features and sky subtraction errors in the near IR. Redshifts were measured by cross correlation analysis with AGN and galactic templates, using the IRAF RVSAO package. A few identifications are based only on the MgII $\lambda 2798$ line, but in each case the proposed z is the only plausible value, given the absence of other expected strong lines. Several of our objects are continuum dominated with very faint line features, for these the substantial light grasp of the HET was important. All of the observed targets were found to be AGN, although some spectra were taken under rather

poor conditions. Some of these have relatively uncertain z estimates, these are noted by (:) in Table 2.

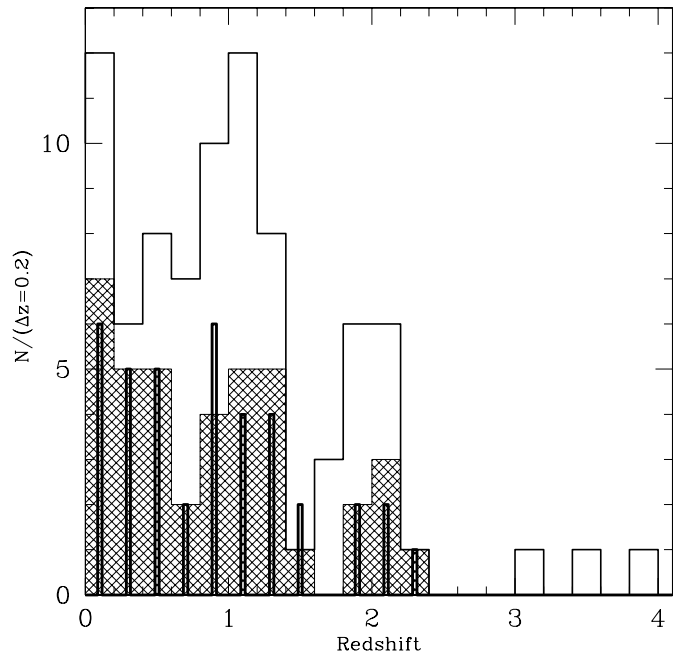


FIG. 6.— The redshift distributions of our Northern blazar sample (solid line histogram), the Northern identifications from the 3EG catalog (shaded histogram) and the Mattox *et al.* (2001) sample (bar histogram).

As of this publication we have obtained 29 new spectroscopic identifications and an additional 16 new associations with previous spectroscopy. The new and archival redshifts for our new blazar IDs are given in Tables 1 and 2. The later table also contains precise positions and sky survey flux estimates; as expected for blazars, the flux at our observation epoch was often substantially different. Most of the AGN were found to be flat spectrum radio quasars. We denote sources with emission line equivalent width $\lesssim 5\text{\AA}$ as BL Lacs. Several sources have the narrow lines (FWHM < 1000km/s) and lower excitation states characteristic of radio galaxies, we denote these as ‘R’ in Table 1. It should be noted that within the classical AGN paradigm, narrow-line radio galaxies would not be expected to show blazar activity. The redshift distribution of our identified sources is shown in Figure 6. For comparison, we also plot the redshift distributions of the sources selected by the 3EG and Mattox *et al.* (2001) criteria. The z distributions are rather similar, largely displaying spectroscopic ID selection effects, but it is clear that we have substantially higher sensitivity to high redshift and have nearly doubled the maximum z value.

4. NOTES ON INDIVIDUAL SOURCES

3EG J0118+0248 As noted above, the Mattox *et al.* (2001) identification with the bright steep spectrum source 3C37 is not supported by our analysis and the 3EG association with 0119+041, is apparently superseded (or at least augmented) by our discovery of two flat spectrum candidates along the error ellipse major axis. If these contribute similarly to the γ -ray flux, they would represent extrema of the γ -ray blazar population, with a factor of $\sim 10^4$ difference in luminosity. If the association is confirmed, J0122+0310 at $z=4.0$ would be the highest redshift

non-GRB γ -ray source known. This 3EG source will be particularly interesting for study in the GLAST era, since with higher angular resolution the contributions of the several posited associations can be disentangled and GLAST's good sensitivity above 10GeV should allow intergalactic absorption of J0122+0310 against a cosmic background of starlight to be detected at $\gtrsim 20$ GeV.

3EG J0204+1458 In addition to the likely association J0204+1514 this source may also incorporate flux from the flatter and more centrally placed radio source J0205+1444.

3EG J0215+1123 with a reasonably large FoM J0213+1213 is an interesting low z BL Lac candidate for TeV studies.

3EG J0222+4253 This object has been argued to be a composite by Kuiper *et al.* (2000) with a possible pulsed detection of the millisecond pulsar PSR J0218+42 accounting for part of the sub-GeV flux. The remainder was attributed (also in the 3EG catalog) to the BL Lac 3C 66A. This source, with $\alpha_{1.4/8.4} = 0.62$, lies just below the spectral cut-off for inclusion in our FoM. However, 2.3 GHz VLBA data are available (Fey & Charlot 2000) which give a much flatter index for the compact component, which we adopt in Table 1. This does make 3C 66A highly likely. CLASS analysis also selects the 215mJy source J0223+4259 (3C 66B, a radio galaxy with a core+jet at $z = 0.02$) as a plausible counterpart. Confusion in the NVSS image prevents detection of the core, so using the 15GHz core flux measured by Jackson, *et al.* (1993) we obtain $\alpha_{8.4/15} = 0.38$ and a strong plausible association. The GeV localization of Kuiper *et al.* (2000) supports either 3C object as the source of the higher energy γ -rays. Certainly GLAST observations will be helpful sorting out this complex region. Interestingly, a TeV detection is claimed in this region Neshpor *et al.* (1998) which would be somewhat surprising from z as large as 0.44. The apparent position is consistent with either 3C 66A or 3C 66B and future air Cerenkov observations may be able to select the preferred source, given their $\sim 0.1^\circ$ separation.

3EG J0245+1758 The source closest to the TS maximum is a strong-lined FSRQ at $z=3.59$. This source shows a likely damped Ly α system at $z \approx 3.15$, raising the possibility that the source is gravitationally magnified by an intervening Galaxy.

3EG J0329+2149 Mattox *et al.* (2001) noted the radio source as a possible association. We confirm it as a likely blazar counterpart and have measured $z=2.07$, in agreement with Halpern, Eracleous & Mattox (2003).

3EG J0404+0700 The better of the two likely associations is our most puzzling case, spectroscopically. When first observed, the spectrum was highly continuum dominated. The two strongest lines were picked up as Ly α and CIV $\lambda 1449$ at $z = 3.13$ in cross-correlation analysis. Both are (local) $\gtrsim 5\sigma$ detections; they have rest equivalent widths of 0.44\AA and 0.39\AA , respectively. CIII $\lambda 1909$ is obscured due to the fringing and no other strong lines are expected. This redshift ID is supported by an apparent strong MgII absorption doublet at $z = 1.578$ (REW $0.19/0.22\text{\AA}$). With such low EW for the emission lines this source is (in this state) clearly a BL Lac (Marcha *et al.* 1996). However a second observation several months later caught the source in a low state for which broad MgII

line and several Ne and O lines give a highly significant measurement of $z = 1.133$. The MgII line is in fact also present in the high state at identical flux. The difference spectrum shows no MgII line, but does have the higher z features noted above. We conservatively adopt the lower redshift, as $z = 3.13$ more than doubles that of the highest z BL Lac cataloged to date (PKS 1309-216 $z = 1.49$ Blades, Murdoch & Hunstead 1980). Further spectroscopy in a variety of flux states is certainly warranted.

3EG J0450+1105 Halpern, Eracleous & Mattox (2003) have observed J0449+1121, identified in the 3EG catalog as the likely counterpart, and have not confirmed the catalog z . Their nearly featureless spectrum suggests a BL Lac.

3EG J0459+3352 This Galactic error region has at least two maxima. The blazar candidate J0503+3404 is well associated with one peak, but the second peak, nearly 2 degrees away is more likely Galactic.

3EG J0634+0521 This source has been plausibly associated with the Be X-ray binary SAX J0635+0533 (Kaaret 2001), so it might be classified as 'p'.

3EG J0808+5114 This source is probably composite with two likely counterparts (Figure 3).

3EG J0917+4427 The bright, 1.3Jy, flat spectrum association is only plausible, being just outside the 99% contour. However, this error region is highly elongated and source is offset in the short direction. If an unmodeled systematic of $\sim 0.3^\circ$ induces this offset, this would be a likely association.

3EG J1133+0033 and **3EG J1329+1708** we have observed a plausible radio source in each, identifying them as featureless BL Lacs, but have not obtained redshifts.

3EG J1605+1553 Our new identification at $z=0.11$ is brighter at 8.4GHz and has a smaller ΔTS than the association proposed by Mattox *et al.* (2001).

3EG J1621+8203 Mukherjee *et al.* (2002) have previously argued for identification with this Seyfert.

3EG J1835+5918 This source has been the subject of intense study (Reimer *et al.* 2001; Halpern *et al.* 2002), who have both argued that it is an isolated Geminga-like pulsar.

3EG J2016+3657 This crowded Galactic error region contains the SNR CTB 87, several bright HII regions in addition to the radio source B2013+370, claimed as a possible BL Lac (Halpern *et al.* 2001). Our spectrum of this source, taken under very poor conditions, is sufficient to support the continuum-dominated nature of the heavily absorbed counterpart, but is insufficient to determine a redshift. We tentatively adopt the blazar designation of these authors, but confirmation requires improved angular resolution and possibly variability correlation with GLAST.

3EG J2021+3651 Is likely associated with the newly discovered pulsar and plerion discussed in Roberts *et al.*, (2002); Roberts, Romani & Kawai (2001).

3EG J2035+4441 May be associated with an X-ray/radio plerion (Roberts, Romani & Kawai 2001).

3EG J2036+1132 Our analysis produces FoM=0.22 for B2032+107 (a $z = 0.6$ BL Lac), the 3EG A designated counterpart of this source. This is just below our cutoff, but as it is significantly less than the FoM of J2034+1154, we propose re-assignment to this source.

Our second source J2031+1219 is bright and flat, but lies significantly outside the 99% confidence contour. A re-evaluation of the likelihood contours in terms of multiple sources could affect the rankings of these plausible counterparts.

3EG J2206+6602 The 3EG catalog also selected this source with low probability; we confirm it as a $z = 1.12$ FSRQ.

3EG J2209+2401 This source was claimed as an identification in (Mattox *et al.* 2001), but the listed redshift was evidently a typographical error, repeating that of another source. We have measured a single line z that excludes the published result.

3EG J2227+6122 This source is likely identified with the recently discovered X-ray/radio pulsar PSR J2229+6114 and its associated wind nebula (Halpern *et al.* 2001b).

5. CONCLUSIONS AND IMPLICATIONS

We believe that we have made a relatively unbiased assessment of the association of flat spectrum radio sources with *EGRET* AGN, identifying plausible counterparts down to 8.4GHz fluxes of ~ 100 mJy. Assuming, as we have argued, that the bulk of our likely and plausible IDs are correct, we have substantially increased the completeness of identification of the Northern $|b| \geq 10^\circ$ *EGRET* sources from $\sim 40\%$ to $\sim 70\%$. We have also argued that in a number of instances the 3EG sources are composites; including this, the increase in the number of proposed γ -ray blazars is even larger.

Our identification allows selection of sources with substantially smaller 8.4GHz radio flux. It should not be too surprising that the number of candidates tapers off smoothly below the previous typical 1Jy value. We suspect that with smaller GLAST error ellipses or improved multi-wavelength constraints, identification could continue well below the ~ 0.1 Jy limit of our survey. Our identification of ~ 30 sources that have flat spectrum counterparts (if any) well below 0.1Jy does not, of course, preclude that some of these may be radio-faint or steep spectrum AGN. Indeed, excess coincidences do continue slightly below our FoM identification limit (Figure 2). Also a number of the 3EG and Mattox *et al.* (2001) identifications not duplicated here are steep spectrum, but very bright low z AGN. In these cases (with the exception of 3EG J0118+0248/3C037, discussed above) the steep spectrum proposed counterpart is located at large ΔTS . Nevertheless, if such sources are truly associated, it is reasonable that these form a distinct subset of the 3EG population, not identified in this analysis. However, the fact that an appreciable fraction of the ‘non-blazar’ 3EG sources correlate with the Galactic disk suggests that many represent a new (old) Galactic population. Detailed assessment of the completeness of blazar IDs through the plane requires careful treatment of the 3EG exposure maps; we defer this and other population analysis to a later paper.

Along with fainter radio associations, we have pushed

back the horizon of plausible blazar identifications (Figure 4). It will be interesting to compare the SED and VLBI β_\perp properties of these fainter blazar counterpart candidates. This survey has found several individual targets of particular interest, including good γ -ray source associations at $z = 3 - 4$, several distant BL Lacs, and several low z AGN that may be suitable targets for ground-based TeV observations. These targets should be the blazars brightest to GLAST and they will provide the most detailed spectra and light curves; as such they merit further study in preparation for the GLAST era. Since spectroscopic identifications are continuing, we defer detailed discussion of the red shift/ luminosity function distributions to a future paper.

The ‘non-blazars’ are also excellent targets for further study in preparation for GLAST, since this sample will most likely produce new classes of high energy emitters. While we do not discuss here the correlation of γ -ray spectra and variability with the lower energy SEDs, we do note that our ‘non-blazars’ correlate fairly well with the ‘steady’ sources of Gehrels, *et al.* (2000) and the ‘persistent’ sources of Grenier (2000), although exceptions occur. Clearly, pushing the improved identifications south to cover the Galactic bulge and beyond will be very important for characterization of these populations.

We thank Roger Blandford for helpful discussions on the nature of γ -ray blazar sources and for assistance with access to the CLASS source list. Ian Browne and Thomas York are also thanked for passing along an early copy of these important data. The referee, R.C. Hartman, and S. Digel provided careful readings and comments that substantially improved the manuscript.

We are particularly grateful to the HET team, especially Gary Hill for bringing the Marcario LRS into operation and Matt Shetrone, Jeff Mader, Brian Roman and the rest of the telescope team for getting these early observations done. We dedicate these HET results to the late Stanford provost Gerald J. Lieberman, whose early support of Stanford’s participation in the HET made this project possible.

The Hobby-Eberly Telescope is operated by McDonald Observatory on behalf of The University of Texas at Austin, the Pennsylvania State University, Stanford University, Ludwig-Maximilians-Universität München, and Georg-August-Universität Göttingen. The Marcario Low Resolution Spectrograph is a joint project of the Hobby-Eberly Telescope partnership and the Instituto de Astronomía de la Universidad Nacional Autónoma de México.

This research has made use of the NASA/IPAC Extragalactic Database (NED) which is operated by the Jet Propulsion Laboratory, California Institute of Technology, under contract with the National Aeronautics and Space Administration. DSE was supported by SLAC under DOE contract DE-AC03-76SF00515 and PFM acknowledges support from NASA contract NAS5-00147.

REFERENCES

- Blades, J.C., Murdoch, H.S. & Hunstead, R.W. 1980, MNRAS, 191 61.
- Condon, J.J., *et al.* 1991, AJ, 102, 2041
- Fey, A.L. & Charlot, P. 2000, ApJS, 128, 17
- Gehrels, N., *et al.* 2000, *Nature*, 404, 363
- Grenier, I.A. 2000, A&A, 364, L93
- Halpern, J.P., Eracleous, M., Mukherjee, R., Gotthelf, E.V. 2001, ApJ, 551, 1016
- Halpern, J.P., *et al.* 2001, ApJ, 552, L125
- Halpern, J.P., Gotthelf, E.V., Mirabal, N. & Camilo, F. 2002, ApJ, 573, L41
- Halpern, J.P., Eracleous, M. & Mattox, J.R. 2003, AJ, in press.
- Hartman, R.C., *et al.* 1999, ApJS, 123, 79
- Hill, G.J., Nicklas, H.E., MacQueen, P.J., Tejada, C., Cobos Duenas, F.J. & Mitsch, W. 1998 Proc. SPIE, 3355, 375
- Jackson, N., Sparks, W.B., Miley, G.K. & Machetto, F. 1993, A&A, 269, 128
- Kaaret, P. & Cottam, J. 1996, ApJ, 462, 35
- Kaaret, P. 2001, *Ast.Sp.Sci.Lib*, 267, 191
- Kuiper, L. *et al.* 2000, A&A, 359, 615.
- Landt, H., *et al.* 2001, MNRAS, 323, 757.
- Marcha, M.J.M., Browne, I.W.A., Impey, C.D. & Smith, P.S. 1996, MNRAS, 281, 425
- Mattox, J.R., *et al.* 1996, ApJ, 461, 396
- Mattox, J.R., Hartman, R.C., Reimer, O. 2001, ApJS, 135, 155
- Monet, D.G. *et al.* 2003, AJ, 125, 984
- Mukherjee, R., Halpern, J., Mirabal, N. & Gotthelf, E.V. 2002, ApJ, 574, 693
- Neshpor, Y.-I., *et al.* 1998, *AstL*, 24, 134.
- Myers, S.T., Jackson, N.J., Browne, I.W.A., Bruyn, A.G., Pearson, T.J., Readhead, A.C.S., Wilkinson, P.N., Biggs, A.D., Blandford, R.D., Fassnacht, C.D., Koopmans, L.V.E., Marlow, D.R., McKean, J.P., Norbury, M.A., Phillips, P.M., Rusin, D., Shepherd, & M.C., Sykes, C.M. 2002, astro-ph/0211073
- Ramsey, L. W. *et al.* 1998, Proc. SPIE, 3352, 34
- Reimer, O. *et al.* 2001, MNRAS, 324, 772
- Roberts, M.S.E. *et al.*, 2002, ApJ, 577, 19
- Roberts, M.S.E., Romani, R.W. & Kawai, N. 2001, ApJS, 133, 451
- Urry, C.M. & Padovani, P. 1995, PASP, 107, 803
- Urry, C.M., 1999, *Astpart. Phys.*, 11, 159.
- Veron-Cetty, M.P., Veron, P. 2001, A&A, 374, 92
- Wallace, P.M., Halpern, J.P., Magalhaes, A.M., Thompson, D.J. 2002, ApJ, 569, 36
- White, R.L. & Becker, R.H. 1992, ApJS, 79, 331.
- Yadigaroglu, I.-A. & Romani, R.W. 1997, ApJ, 476, 347.

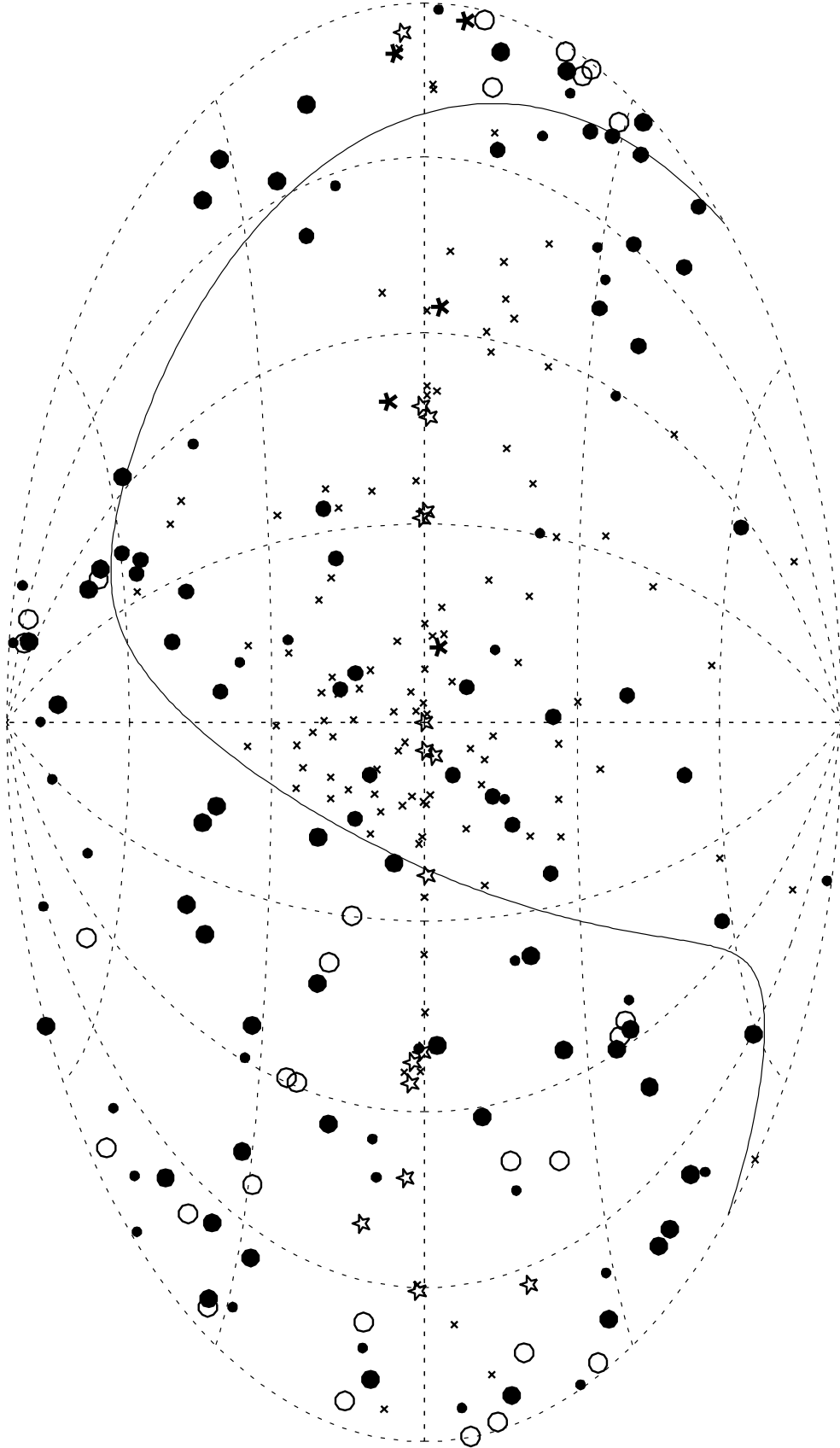


FIG. 4.— Aitoff equal area projection of 3EG sources in Galactic coordinates, showing our new classifications in the Northern hemisphere. Large filled circle=high confidence blazar, Smaller filled circle=plausible blazar, Filled star=pulsar, Open star=pulsar/plerion candidate, Open circle= Non-Blazar, cross=presently unclassified. Symbols south of $\text{DEC}=0^\circ$ are similar, with AGN drawn from the 3EG A/a classifications.

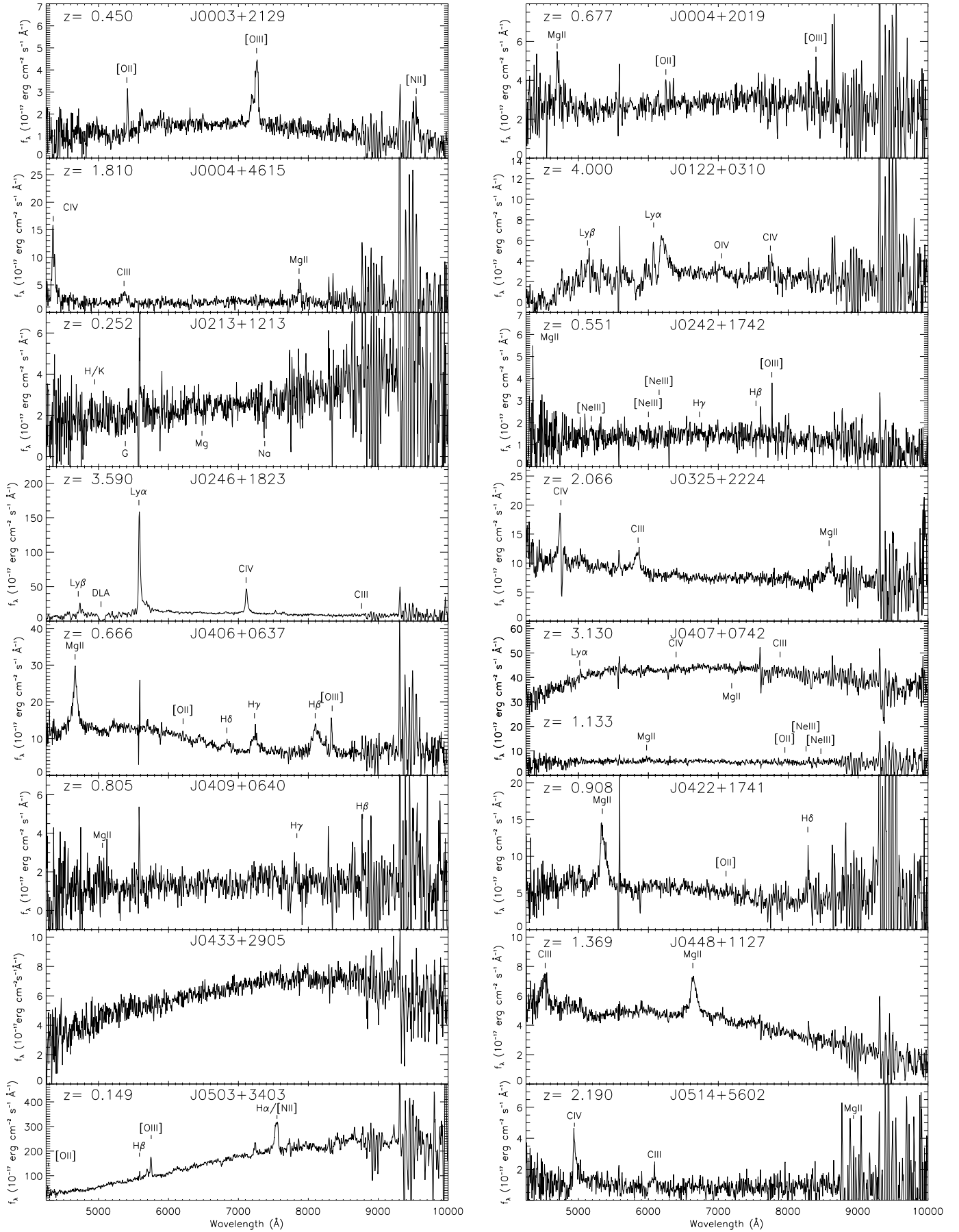


FIG. 5.— HET/Marcario LRS spectra.

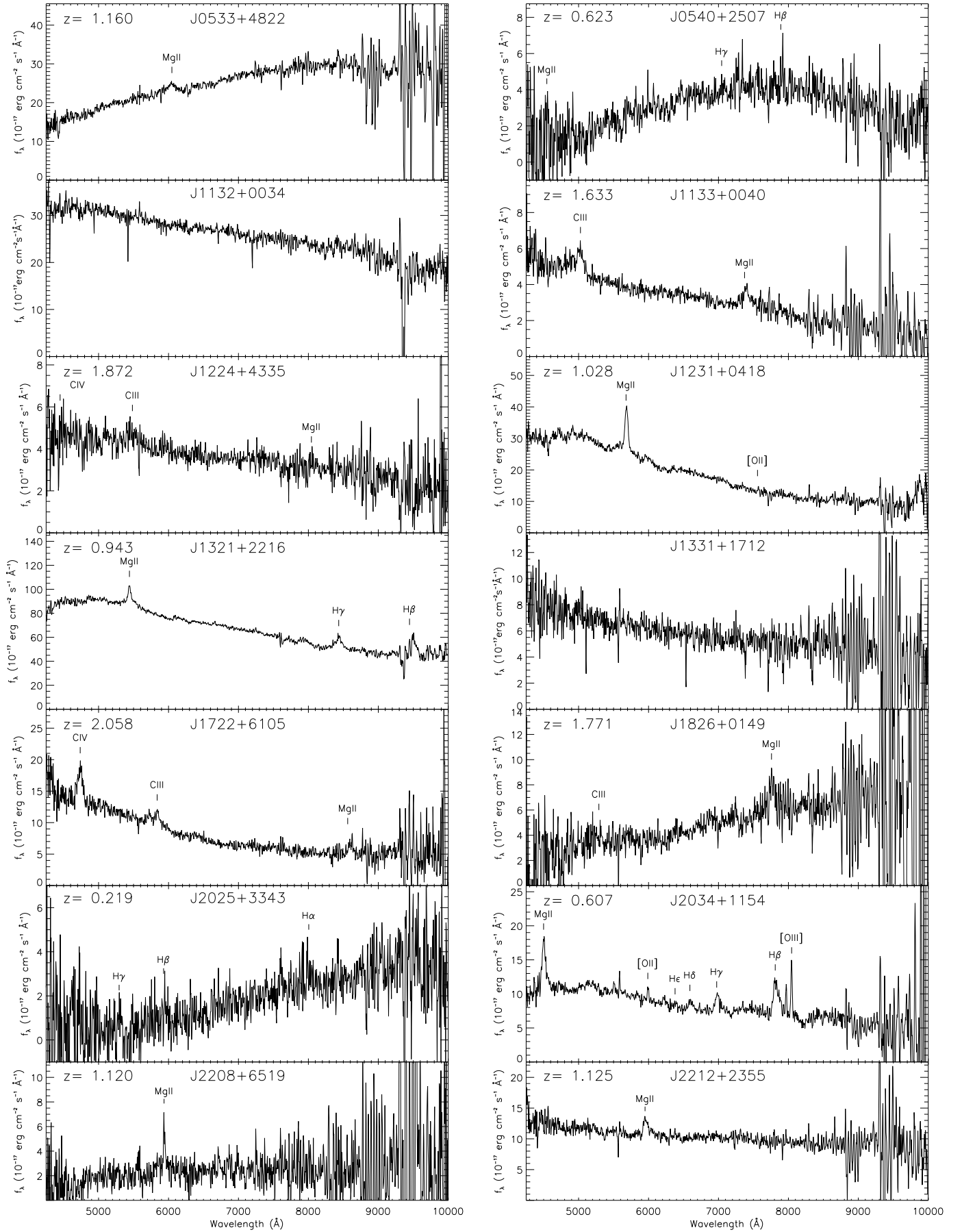


FIG. 5.— (continued) HET/Marcario LRS spectra.

TABLE 1
NORTHERN 3EG OBJECTS

3EG	ID	$S_{s,4}$	α	FoM	z	Notes				
J0010+7309	CTA1									pN
J0118+0248	J0113+0222	644	-0.1	3.55	0.05	†				R
	J0122+0310	121	-0.1	0.59	4.00	*				f
	J0121+0422,0119+041 (0115+027,3C037)	1351	-0.1	0.29	0.63				a	f
		—			0.67			—		
J0204+1458	J0204+1514,0202+149	3325	0.09	5.77	0.41			+	A	f
	J0205+1444	185	0.01	2.58	—	*				
J0215+1123	J0213+1213	164	-0.1	0.53	0.25	*				b
J0222+4253	PSR J0218+4232 J0222+4302,0219+428,3C66A	728	0.17	3.16	0.44			+	A	pb? b
	J0223+4259,3C 66B	215	0.38	0.90	0.02	†				R
J0229+6151										G
J0237+1635	J0238+1636,0235+164	5453	-0.5	4.33	0.94			+	A	f
J0239+2815	J0237+2848,0234+285	3123	-0.1	0.58	1.21			+	A	f
J0241+6103	LSI +61 303									pN
J0245+1758	J0242+1742	236	-0.1	1.64	0.55	*				f
	J0246+1823	125	0.29	0.42	3.59	*				f
J0323+5122										G
J0329+2149	J0325+2224,0322+222	528	-0.0	1.40	2.07	*		—		f
J0348+3510										N
J0404+0700	J0406+0637	227	-0.0	1.11	0.67	*				f
	J0407+0742	524	-0.3	3.01	1.13	*				b
	J0409+0640	181	-0.1	0.93	0.81	*				f
J0407+1710										N
J0416+3650									a	G
	(0415+379,3C111)	—			0.05					
J0423+1707	J0422+1741	131	-0.5	0.78	0.91	*				f
J0426+1333										N
J0429+0337										N
J0433+2908	J0433+2905,0430+2859	432	-0.0	6.15	—			—	A	b
J0435+6137										N
J0439+1555										N
J0439+1105										N
J0450+1105	J0448+1127	206	0.17	0.54	1.37	*				f
	J0449+1121,0446+112	1226	-0.2	3.58	1.2?			—	A	?
J0459+0544	J0457+0645	434	0.07	0.30	0.41	†				f
	J0502+0609,0459+060	543	0.28	0.85	1.11			—	A	f
	J0505+0459	808	0.10	0.81	0.95	†				f
J0459+3352	J0503+3403	448	0.38	0.59	0.15	*				R?
J0500+2529										N
	(0459+252)	—			0.28			—		R
J0510+5545	J0514+5602	229	0.18	0.41	2.19	*				f
J0516+2320	SolarFlare									S
J0520+2556										N
J0521+2147										N
J0530+1323	J0530+1331,0528+134	3074	-0.3	6.36	2.07			+	A	f
J0533+4751	J0533+4822,0529+4820	556	-0.1	4.23	1.16	*		—		f
J0534+2200	Crab									P
J0542+2610	J0540+2507	207	0.12	0.63	0.62	*				f
J0546+3948										
J0556+0409										N
J0613+4201										N
J0617+2238	IC443									p
J0628+1847										G
J0631+0642										G
J0633+1751	Geminga									P
J0634+0521										G
J0721+7120	J0721+7120,0716+714	594	0.09	7.67	—			+	A	b
J0737+1721	J0738+1742,0735+178	2942	-0.1	12.58	0.42			+	A	b
	J0739+1739	114	-0.2	0.63	—	*				
J0743+5447	J0742+5444,0738+5451	142	0.36	0.56	0.72			—	A	f
J0808+4844										N
	(0804+499)	880	0.12	0.10	1.43				a	f
	(0809+483,3C196)	—			0.87			—	a	
J0808+5114	J0807+5117,0803+5126	358	-0.4	8.32	1.14				a	f
	J0809+5218	154	0.08	1.24	0.14	†				b
J0828+0508	J0831+0429,0829+046	1225	-0.0	3.39	0.18			+	A	b
J0829+2413	J0830+2410,0827+243	713	0.00	6.41	0.94			+	A	f
J0845+7049	J0841+7053,0836+710	1757	0.42	1.14	2.22			+	A	f
J0853+1941	J0854+2006,0851+202	2997	-0.3	7.48	0.31			+	A	b
J0910+6556										N
J0917+4427	J0920+4441,0917+449	1368	-0.1	0.49	2.18				a	f
J0952+5501	J0957+5522,0954+556	1498	0.39	0.49	0.90			+	A	f
J0958+6533	J0958+6533,0954+658	1269	-0.3	13.14	0.37			+	A	b
J1009+4855										N
	(1011+496)	252	0.21	0.24	0.20				a	b
J1052+5718	J1058+5628,1055+567	189	0.09	0.42	0.14				a	b
J1104+3809	J1104+3812,Mrk 421,1101+384	631	-0.0	8.52	0.03			+	A	b
J1133+0033	J1132+0034	213	0.42	0.71	—	*				b
	J1133+0015	119	0.35	0.42	1.17	†				f
	J1133+0040	320	0.05	4.07	1.63	*				f

TABLE 1—*Continued*

3EG	ID	$S_{8.4}$	α	FoM	z	Notes			
J1200+2847	J1159+2914,1156+295	1233	0.24	0.98	0.73		+	A	f
J1212+2304									N
J1222+2315									N
J1222+2841	J1221+2813,1219+285	1217	-0.2	0.34	0.10		-	A	b
J1224+2118	J1224+2122,1222+216	1073	0.34	1.97	0.44		+	A	f
J1227+4302	J1221+4411	435	0.12	0.49	1.35	†			f
	J1224+4335	220	0.26	0.91	1.87	*			f
	J1226+4340	145	0.10	0.95	—	*			
J1229+0210	J1229+0203,3C273,1226+023	41725	0.04	8.77	0.16		+	A	f
J1235+0233									N
J1236+0457	J1231+0418	302	0.05	1.34	1.03	*			f
	J1239+0443,1237+0459	290	0.09	0.96	1.75			a	f
J1308+8744									N
J1323+2200	J1321+2216	323	-0.0	0.54	0.94	*			f
	J1322+2148	147	0.26	0.29	—	*			
	J1327+2210,1324+224	2107	-0.5	0.75	1.40			a	f
J1329+1708	J1331+1712	120	0.21	0.45	—	*			b
	J1333+1649,1331+170	483	-0.1	2.08	2.09		-	A	f
J1337+5029									N
J1347+2932	J1343+2844	192	0.13	0.34	0.91	†			f
J1424+3734	J1419+3821	775	-0.1	0.90	1.83	†			f
	J1420+3721	158	0.06	0.25	0.97	†			f
	J1421+3855	132	-0.2	0.46	0.49	†			f
	J1426+3625	613	-0.2	0.44	1.09	†			f
J1605+1553	J1603+1554	256	-0.5	4.46	0.11	†			f
	(1604+159)	223.5	0.56	0.00	0.36		-	a	b
J1608+1055	J1608+1029,1606+106	1805	-0.1	3.37	1.23		+	A	f
J1614+3424	J1613+3412,1611+343	3042	0.13	2.14	1.40		+	A	f
J1621+8203	J1632+8232,NGC6251	738	0.05	1.63	0.02				R
J1635+3813	J1635+3808,1633+382	2448	0.04	3.94	1.81		+	A	f
J1727+0429	J1728+0427,1725+044	622	0.04	6.30	0.29		-	A	f
J1733+6017	J1722+6105	203	-0.1	0.95	2.06	*			f
	J1724+6055	166	0.17	0.61	—	*			
J1738+5203	J1740+5211,1739+522	1318	-0.2	11.25	1.38		+	A	f
J1822+1641									N
J1824+3440	J1826+3431	289	0.25	1.11	1.81	†			f
J1825+2854									N
	(1829+2905)	722	0.78	0.00	0.84		-		
J1828+0142	J1826+0149	725	-0.2	1.39	1.77	*			f
J1835+5918									N
J1850+5903									N
J1856+0114	W44/PSR 1853+01								pN
J1903+0550									G
J1928+1733									
J1958+2909									G
J1959+6342	J2006+6424,2005+6416	958	-0.3	2.99	1.57		-		f
J2016+3657									b
J2020+4017	γ Cygni								p
J2021+3716	PSR2021+3651								p
J2022+4317									
J2027+3429	J2025+3343	2728	-0.4	2.85	0.22	*			f
J2033+4118									
J2035+4441	RRK								p
J2036+1132	J2031+1219	1178	-0.1	0.26	1.22	†			f
	J2034+1154	216	0.24	0.61	0.61	*			f
	(2032+107)	463	0.46	0.22	0.60		-	A	b
J2046+0933	J2049+1003	888	-0.6	3.39	—	*			
J2100+6012	J2102+6015	164	0.35	0.41	—	*			
	(2105+598)	179	0.57	0.00	—			a	
J2202+4217	J2202+4216,BL Lac,2200+420	3321	0.31	3.44	0.07		+	A	b
J2206+6602	J2208+6519,2206+650	249	0.33	0.41	1.12	*		a	f
J2209+2401	J2212+2355,2209+236	719	-0.1	4.11	1.13	*	+	A	f
J2227+6122	PSR J2229+6114								p
J2232+1147	J2232+1143,CTA 102,2230+114	2923	0.48	0.92	1.04		+	A	f
J2243+1509									N
J2248+1745									N
J2254+1601	J2253+1608,3C 454.3,2251+158	10380	0.10	8.57	0.86		+	A	f
J2255+1943	J2253+1942,2250+1926	362	-0.1	4.46	0.28			a	f
J2314+4426									N
J2352+3752									N
	(2346+385)	243	0.22	0.24	1.03			a	
J2358+4604	J0004+4615	214	-0.3	0.28	1.81	*			f
	J2354+4553,2351+456	990	0.34	0.67	1.99		-	A	f
J2359+2041	J0001+1914	504	-0.3	0.29	3.10	†			f
	J0003+2129	269	-0.6	1.69	0.45	*			f
	J0004+2019	162	-0.6	1.17	0.68	*			f
	J2358+1955,2356+196	558	0.10	1.44	1.07		-	A	f

Note. — Column 7: Our new associations and/or redshifts * = new spectral ID. † = redshift from NED, 10th QSO Catalog, etc.

Column 8: Mattox *et al.* (2001) selected blazars +=‘High probability’, -=‘Plausible’

Column 9: 3rd *EGRET* Catalog blazars, A=‘High confidence’, a=‘lower confidence’

Column 10: classification f=FSRQ, b=BL Lac, R=narrow-line radio galaxy, G=Likely galactic, N=‘Non-blazar’, p=Pulsar candidate/plerion, P=confirmed pulsar.

TABLE 2
NEW 3EG COUNTERPART CANDIDATES WITH SPECTROSCOPIC IDENTIFICATION

ID	FoM	α (J2000 Coordinates)	δ	R2 Magnitude	B2 Magnitude	z	Type
J0001+1914	0.29	00 01 08.623	+19 14 33.82	20.50	21.19	3.100	f
J0003+2129	1.69	00 03 19.348	+21 29 44.42	19.75	21.10	0.450*	f
J0004+2019	1.17	00 04 35.757	+20 19 42.25	20.25	20.81	0.677*	f
J0004+4615	0.28	00 04 16.128	+46 15 17.96	20.44	20.53	1.810*	f
J0113+0222	3.55	01 13 43.145	+02 22 17.32	11.22	11.55	0.047	R
J0122+0310	0.59	01 22 01.911	+03 10 02.43	20.07	20.91	4.000*	f
J0213+1213	0.53	02 13 05.184	+12 13 10.90	19.75	21.15	0.252:*	b
J0223+4259	0.90	02 23 11.407	+42 59 31.43	—	—	0.021	R
J0242+1742	1.64	02 42 24.268	+17 42 58.85	20.28	21.31	0.551:*	f
J0246+1823	0.42	02 46 11.823	+18 23 30.08	19.5	20.94	3.590*	f
J0325+2224	1.40	03 25 36.814	+22 24 00.42	19.14	20.17	2.066*	f
J0406+0637	1.11	04 06 34.308	+06 37 14.97	19.47	19.35	0.666*	f
J0407+0742	3.01	04 07 29.087	+07 42 07.45	17.28	17.59	1.133*	b
J0409+0640	0.93	04 09 25.847	+06 40 35.09	—	—	0.805*	f
J0422+1741	0.78	04 22 47.774	+17 41 15.88	19.49	19.74	0.908*	f
J0448+1127	0.54	04 48 50.413	+11 27 54.40	18.83	20.42	1.369*	f
J0457+0645	0.30	04 57 07.710	+06 45 07.27	18.14	19.33	0.405	f
J0503+3403	0.59	05 03 56.786	+34 03 28.14	17.30	18.99	0.149*	R?
J0505+0459	0.81	05 05 23.187	+04 59 42.73	17.58	17.24	0.954	f
J0514+5602	0.41	05 14 18.698	+56 02 11.05	—	—	2.190*	f
J0533+4822	4.23	05 33 15.864	+48 22 52.82	18.25	20.34	1.160*	f
J0540+2507	0.63	05 40 14.345	+25 07 55.35	—	—	0.623:*	f
J0809+5218	1.24	08 09 49.189	+52 18 58.25	14.54	15.59	0.138	b
J1132+0034	0.71	11 32 45.619	+00 34 27.82	17.23	17.56	—*	b
J1133+0015	0.42	11 33 03.029	+00 15 48.99	18.89	18.06	1.173	f
J1133+0040	4.07	11 33 20.058	+00 40 52.84	18.88	19.43	1.633*	f
J1221+4411	0.49	12 21 27.045	+44 11 29.67	17.75	18.51	1.345	f
J1224+4335	0.91	12 24 51.507	+43 35 19.28	20.22	19.71	1.872*	f
J1231+0418	1.34	12 31 27.582	+04 18 01.89	17.73	18.08	1.028*	f
J1321+2216	0.54	13 21 11.204	+22 16 12.10	19.37	19.47	0.943*	f
J1331+1712	0.45	13 31 33.446	+17 12 50.62	18.34	18.47	—*	b
J1343+2844	0.34	13 43 00.180	+28 44 07.49	16.75	17.09	0.908	f
J1419+3821	0.90	14 19 46.616	+38 21 48.49	19.25	19.33	1.832	f
J1420+3721	0.25	14 20 00.342	+37 21 34.68	18.23	18.30	0.969	f
J1421+3855	0.46	14 21 06.034	+38 55 22.83	17.39	17.84	0.490	f
J1426+3625	0.44	14 26 37.086	+36 25 09.58	20.27	20.77	1.091	f
J1603+1554	4.46	16 03 38.065	+15 54 02.38	12.15	13.97	0.109	f
J1722+6105	0.95	17 22 40.059	+61 05 59.80	19.42	19.25	2.058*	f
J1826+0149	1.39	18 26 25.066	+01 49 40.12	—	—	1.771*	f
J1826+3431	1.11	18 26 59.982	+34 31 14.10	16.20	17.66	1.814	f
J2025+3343	2.85	20 25 10.940	+33 43 00.21	—	—	0.219:*	f
J2031+1219	0.26	20 31 54.999	+12 19 41.34	17.42	—	1.215	f
J2034+1154	0.61	20 34 37.110	+11 54 31.38	—	17.01	0.607*	f
J2208+6519	0.41	22 08 03.103	+65 19 38.78	—	—	1.120:*	f
J2212+2355	4.11	22 12 05.970	+23 55 40.59	19.69	20.66	1.125*	f

Note. — Some sources have been previously flagged (see Table 1), but are spectroscopically confirmed here. Column: 5,6, USNO B1.0 magnitudes (Monet, *et al.* 2003), Column 7: new(*) or archival z, Column 8: classification (see Table 1).